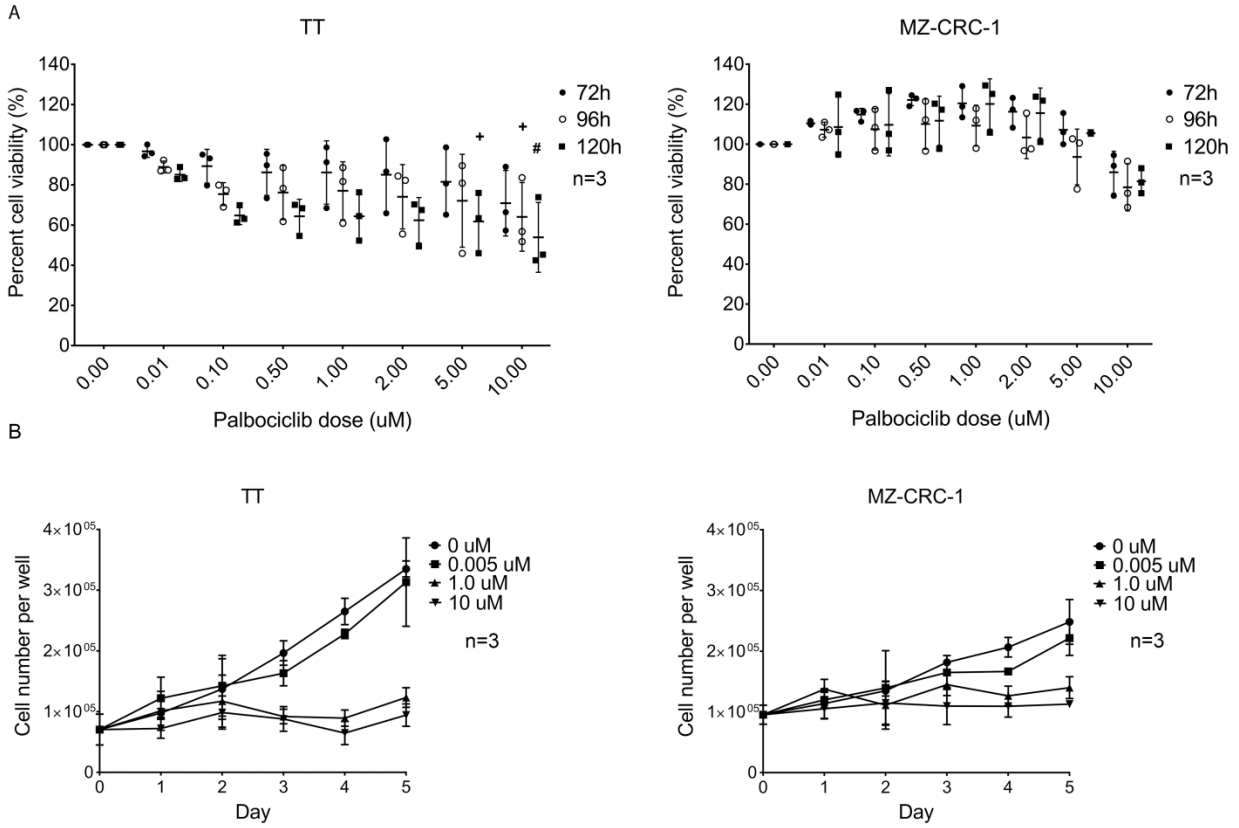

Figure S1. TT and MZ-CRC-1 cell viability and proliferation after Palbociclib treatment. Cell viability assays (**A**) and cell counting assays (**B**) were performed with TT and MZ-CRC-1 cells treated with Palbociclib or vehicle control. WST-8 solution was added at 72h-120h and the optical density was read using a spectrophotometer for viability assays. These data were normalized to the 0µM (vehicle control) wells and represented as percentages. In cell counting assays, the cells were counted for 5 days after treatment, including vehicle control wells at day 0, using the Countess Automated Cell Countess. Each biological replicate was done in triplicate (cell viability assays) or duplicate (cell counting assays), and the error bars represent the standard deviation. Two-way ANOVA tests followed by Holm's procedure were done on both types of assays. In the case of cell counting assays, log2 transformed data was used for statistical analysis. # $P < 0.01$, + $P < 0.05$.

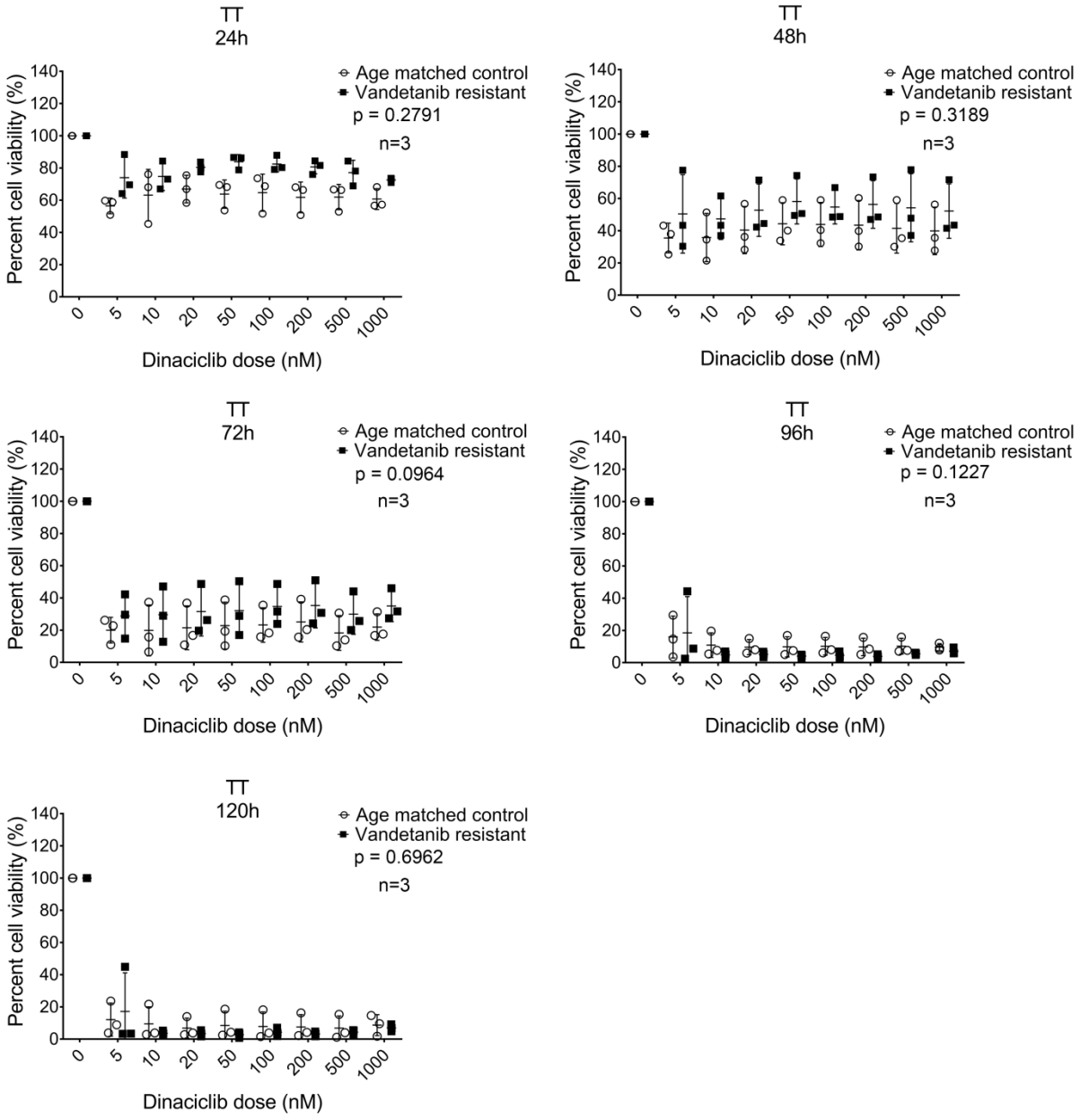

Figure S2. TT Vandetanib-resistant and age-matched controls' viability after Dinaciclib treatment.

Cell viability assays for TT Vandetanib-resistant cells and age-matched controls. The cells were treated with Dinaciclib and incubated for 24-120h. WST-8 solution was added at each time point and the optical density was read using a spectrophotometer. The data are normalized to the 0nM (vehicle control) wells and represented as percentages. Each biological replicate was done in triplicate, and the error bars represent the standard deviation. Linear mixed models were used to statistically analyze the data after log2 transformation.

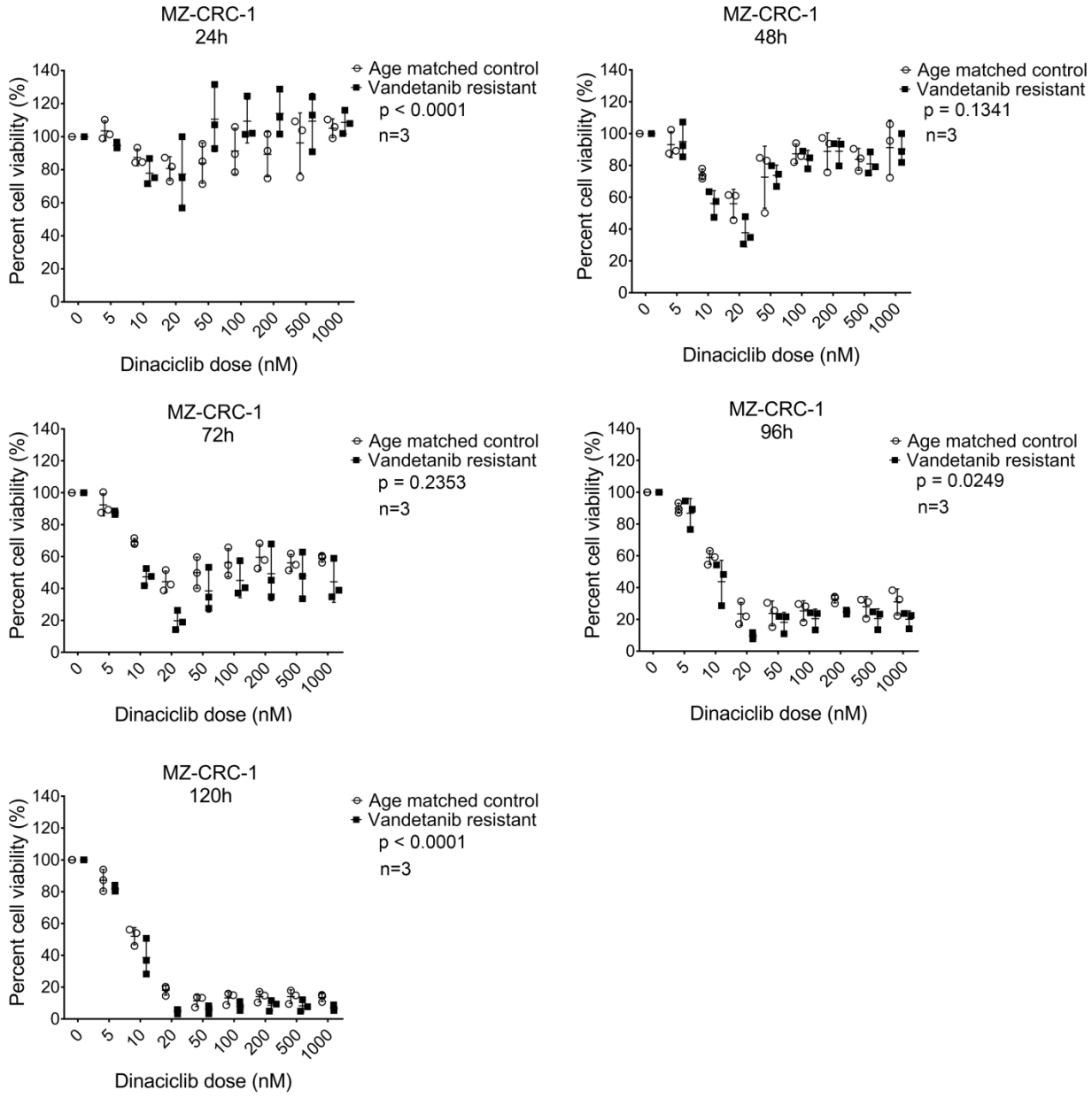

Figure S3. MZ-CRC-1 Vandetanib-resistant and age-matched controls' viability after Dinaciclib treatment.

Cell viability assays for MZ-CRC-1 Vandetanib-resistant cells and age-matched controls. The cells were treated with Dinaciclib and incubated for 24-120h. WST-8 solution was added at each time point and the optical density was read using a spectrophotometer. The data was normalized to the 0nM (vehicle control) wells and represented as percentages. Each biological replicate was done in triplicate, and the error bars represent the standard deviation. Linear mixed models were used to statistically analyze the data after log2 transformation.

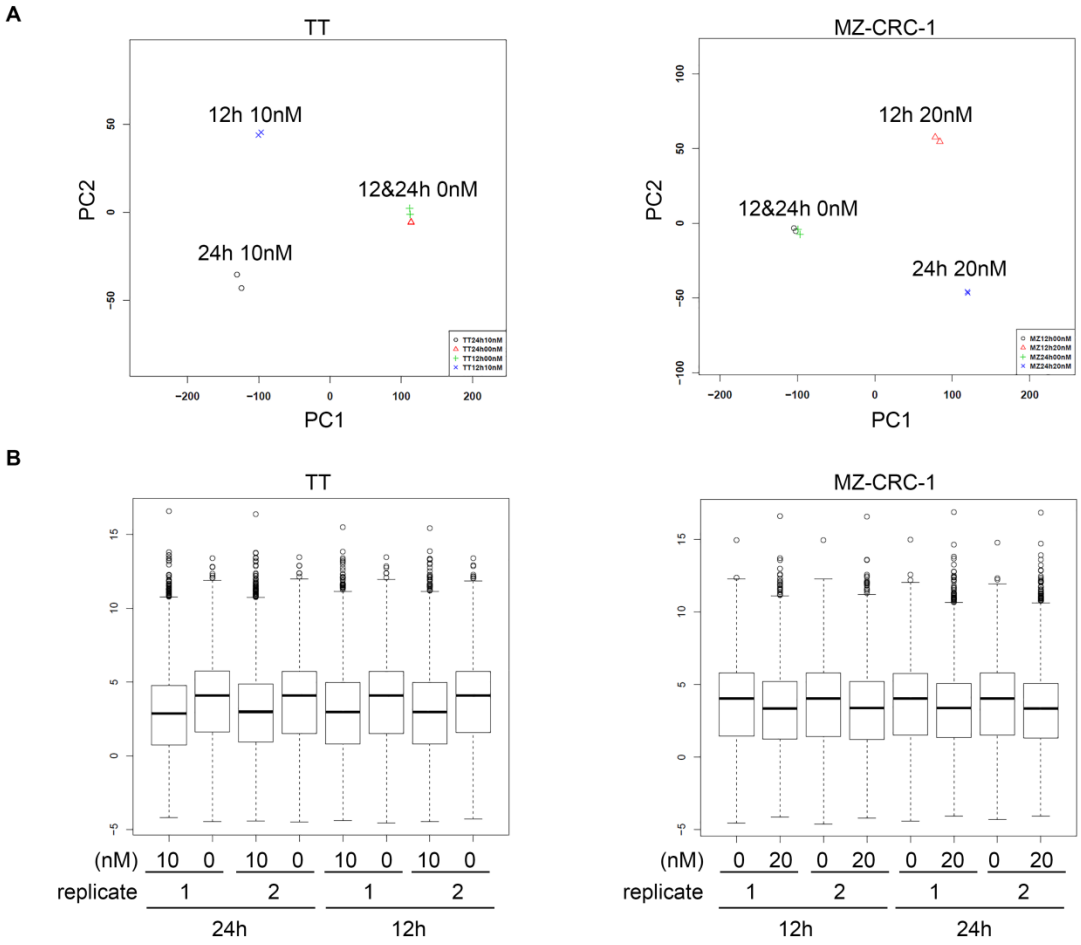

Figure S4. Principal component analysis and mRNA expression profiles.
TT and MZ-CRC-1 cells were treated with vehicle control or Dinaciclib (10nM TT and 20nM MZ-CRC-1) for 12h and 24h; and RNA sequencing was performed. **A.** Principal component plots showing treatment as the variable that is associated with most of the change. **B.** mRNA expression of treated cells was downregulated compared to that of untreated cells for all time points and replicates. Data represents two biological replicates.

Table S1. GSEA results for TT cells after treatment with Dinaciclib.

Upregulated in class	0nM	0nM	0nM	24h_10nM
GeneSet	Reactome Generic_Transcription_Pathway	Fischer_G2_M_Cell_Cycle	Dazard_Response_To_Uv_Nhek_Dn	Reactome_RNA_Pol_I_RNA_Pol_III_and_Mitochondrial_Transcription
Enrichment Score (ES)	0.54585063	0.53538096	0.5405646	-0.5568247
Upregulated in class	0nM	0nM	0nM	24h_10nM
Normalized Enrichment Score (NES)	1.6443505	1.5962245	1.6242611	-3.3080742
Nominal p-value	< 0.001	< 0.001	< 0.001	< 0.001
FDR q-value	0.16338143	0.23976356	0.21791176	< 0.001
FWER p-Value	0.869	0.995	0.952	< 0.001

Table S2. GSEA results for MZ-CRC-1 cells after treatment with Dinaciclib.

Upregulated in class	0nM	0nM	0nM	20nM
GeneSet	Reactome_Mitotic_G1_G1_S_Phases	Fischer_G2_M_Cell_Cycle	Reactome_Dna_Replication	Reactome_RNA_Pol_I_RNA_Pol_III_and_Mitochondrial_Transcription
Enrichment Score (ES)	0.5818768	0.54078984	0.5422023	-0.6687349
Normalized Enrichment Score (NES)	2.1021037	2.056033	2.0360003	-2.998046
Nominal p-value	< 0.001	< 0.001	< 0.001	< 0.001
FDR q-value	0.002205691	0.001763156	0.0022009527	< 0.001
FWER p-Value	0.004	0.008	0.014	< 0.001

Table S3. Top GSEA pathways downregulated in TT cells treated with 10nM Dinaciclib.

NAME	SIZE	ES	NES	NOM p-value	FDR q-value	FWER p-value
Burton_Adipogenesis_1	31	0.676336	1.755451	<0.001	0.244623	0.226
Plasari_Nfic_Targets_Basal_Up	22	0.707376	1.741705	0.001082	0.160152	0.281
Pid_Hedgehog_2pathway	16	0.737296	1.730455	0.001122	0.133235	0.349
Pid_Il3_Pathway	22	0.681504	1.686294	<0.001	0.234699	0.62
Dazard_Response_To_Uv_Scc_Dn	114	0.571397	1.667779	<0.001	0.257552	0.744
Kegg_Basal_Cell_Carcinoma	39	0.624198	1.667392	<0.001	0.21601	0.745
Reactome_G1_S_Specific_Transcription	17	0.712466	1.663837	0.001133	0.198866	0.773
Ly_Aging_Middle_Dn	16	0.714973	1.656882	0.002227	0.198011	0.815
Biocarta_Cellcycle_Pathway	20	0.676472	1.6547	0.001105	0.182877	0.825
Marshall_Viral_Infection_Response_Dn	23	0.666301	1.649676	0.004372	0.178614	0.847
Leonard_Hypoxia	43	0.614268	1.647674	<0.001	0.167661	0.854
Reactome_Generic_Transcription_Pathway	313	0.545851	1.644351	<0.001	0.163381	0.869
Dazard_Response_To_Uv_Nhek_Dn	299	0.540565	1.624261	<0.001	0.217912	0.952
Reactome_Nuclear_Receptor_Transcription_Pathway	39	0.602639	1.62016	<0.001	0.215337	0.966
Pramoonjago_Sox4_Targets_Up	50	0.588401	1.617431	<0.001	0.21138	0.974
Nakayama_Fra2_Targets	36	0.609446	1.60823	0.001041	0.231692	0.986
Gentile_Uv_Response_Cluster_D2	37	0.607627	1.605404	<0.001	0.228164	0.991
Figueroa_Aml_Methylation_Cluster_6_Dn	21	0.650761	1.600146	<0.001	0.236158	0.994
Fischer_G2_M_Cell_Cycle	222	0.535381	1.596225	<0.001	0.239764	0.995
Gyorffy_Doxorubicin_Resistance	44	0.593534	1.583587	<0.001	0.280211	0.998

Table S4. Top GSEA pathways upregulated in TT cells treated with 10nM Dinaciclib.

NAME	SIZE	ES	NES	NOM p-value	FDR q-value	FWER p-value
Reactome_Amyloids	60	-0.85992	-3.85068	<0.001	0	0
Kegg_Systemic_Lupus_Erythematosus	88	-0.77859	-3.82058	<0.001	0	0
Reactome_Rna_Pol_I_Promoter_Opening	49	-0.87092	-3.74511	<0.001	0	0
Reactome_Packaging_Of_Telomere_Ends	38	-0.86396	-3.68124	<0.001	0	0
Reactome_Meiosis	92	-0.6839	-3.61276	<0.001	0	0
Reactome_Meiotic_Recombination	67	-0.79748	-3.60682	<0.001	0	0
Reactome_Rna_Pol_I_Transcription	74	-0.70892	-3.42831	<0.001	0	0
Reactome_Meiotic_Synapsis	58	-0.71034	-3.18792	<0.001	0	0
Reactome_Telomere_Maintenance	65	-0.67979	-3.16756	<0.001	0	0
Reactome_Srp_Dependent_Cotranslational_Protein_Targeting_To_Membrane	107	-0.49535	-3.13828	<0.001	0	0
Reactome_Deposition_Of_New_Cenpa_Containing_Nucleosomes_At_The_Centromere	52	-0.71253	-3.03708	<0.001	0	0
Reactome_Peptide_Chain_Elongation	84	-0.60794	-2.98132	<0.001	0	0
Reactome_Respiratory_Electron_Transport	65	-0.57897	-2.91526	<0.001	0	0
Reactome_Respiratory_Electron_Transport_Atp_Synthesis_By_Chemiosmotic_Coupling_And_Heat_Production_By_Uncoupling_Proteins_	80	-0.55652	-2.898	<0.001	0	0
Reactome_Rna_Pol_I_Rna_Pol_III_And_Mitochondrial_Transcription	107	-0.51584	-2.70685	<0.001	0	0
Pid_Syndecan_1_Pathway	34	-0.62338	-2.57184	<0.001	0	0
Naba_Collagens	26	-0.66886	-2.56778	<0.001	0	0
Kegg_Ribosome	84	-0.52036	-2.56187	<0.001	0	0

Table S5. Top GSEA pathways downregulated in MZ-CRC-1 cells treated with 20nM Dinaciclib.

NAME	SIZE	ES	NES	NOM p-value	FDR q-value	FWER p-value
Gary_Cd5_Targets_Dn	404	0.543062	2.132112	<0.001	0.002209	0.002
Reactome_Mitotic_G1_G1_S_Phases	126	0.581877	2.102104	<0.001	0.002206	0.004
Reactome_G1_S_Transition	105	0.592556	2.101658	<0.001	0.00147	0.004
Reactome_M_G1_Transition	76	0.59834	2.068002	<0.001	0.00193	0.007
Fischer_G2_M_Cell_Cycle	224	0.54079	2.056033	<0.001	0.001763	0.008
Reactome_S_Phase	105	0.573664	2.047676	<0.001	0.001654	0.009
Reactome_Dna_Replication	182	0.542202	2.036	<0.001	0.002201	0.014
Moreaux_Multiple_Myeloma_By_Taci_Dn	164	0.549237	2.035922	<0.001	0.001926	0.014
Martinez_Response_To_Trabectedin_Dn	263	0.527262	2.033448	<0.001	0.001834	0.015
Reactome_Orc1_Removal_From_Chromatin	64	0.615994	2.026094	<0.001	0.001982	0.018
Chiang_Liver_Cancer_Subclass_Unannotated_Dn	184	0.544092	2.025122	<0.001	0.001802	0.018
Reactome_Scfskp2_Mediated_Degradation_Of_P27 _P21	53	0.627951	2.022855	<0.001	0.001743	0.019
Berenjeno_Transformed_By_Rhoa_Up	492	0.505473	2.021262	<0.001	0.001609	0.019
Reactome_Cyclin_E_Associated_Events_During_ G1_S_Transition_	62	0.615761	2.017414	<0.001	0.001573	0.02
Reactome_Mitotic_M_M_G1_Phases	162	0.544143	2.011092	<0.001	0.001615	0.022
Wong_Embryonic_Stem_Cell_Core	324	0.519653	2.007742	<0.001	0.001653	0.024
Schlosser_Myc_Targets_Repressed_By_Serum	154	0.543896	2.006658	<0.001	0.001555	0.024
Schlosser_Myc_Targets_And_Serum_Response_Dn	46	0.638475	2.000816	<0.001	0.001591	0.026
Reactome_Synthesis_Of_Dna	89	0.575937	1.995626	<0.001	0.001798	0.031
Dacosta_Uv_Response_Via_Ercc3_Xpcs_Up	27	0.69419	1.994941	<0.001	0.001708	0.031

Table S6. Top GSEA pathways upregulated in MZ-CRC-1 cells treated with 20nM Dinaciclib.

NAME	SIZE	ES	NES	NOM p-value	FDR q-value	FWER p-value
Reactome_Rna_Pol_I_Promoter_Opening	55	-0.90979	-3.56035	<0.001	0	0
Reactome_Amyloids	64	-0.8851	-3.54191	<0.001	0	0
Kegg_Systemic_Lupus_Erythematosus	91	-0.82412	-3.49586	<0.001	0	0
Reactome_Meiotic_Recombination	75	-0.83914	-3.47384	<0.001	0	0
Reactome_Rna_Pol_I_Transcription	80	-0.81661	-3.42307	<0.001	0	0
Reactome_Packaging_Of_Telomere_Ends	43	-0.87817	-3.27861	<0.001	0	0
Reactome_Meiosis	102	-0.75536	-3.25696	<0.001	0	0
Reactome_Meiotic_Synapsis	65	-0.78403	-3.1779	<0.001	0	0
Reactome_Deposition_Of_New_Cenpa_Containing_ Nucleosomes_At_The_Centromere	57	-0.7787	-3.12083	<0.001	0	0
Reactome_Rna_Pol_I_Rna_Pol_III_And_Mitochondrial _Transcription	113	-0.66873	-2.99805	<0.001	0	0
Reactome_Telomere_Maintenance	70	-0.70418	-2.82449	<0.001	0	0
Acevedo_Liver_Cancer_With_H3k27me3_Dn	153	-0.54872	-2.54715	<0.001	0	0
Reactome_Chromosome_Maintenance	111	-0.57368	-2.50791	<0.001	4.39E-05	0.001
Reactome_Transcription	194	-0.49382	-2.31873	<0.001	2.52E-04	0.006
Reactome_Extracellular_Matrix_Organization	52	-0.59223	-2.3167	<0.001	2.35E-04	0.006
Acevedo_Liver_Cancer_With_H3k9me3_Dn	101	-0.52342	-2.31262	<0.001	2.21E-04	0.006
Naba_Collagens	22	-0.70908	-2.24496	<0.001	4.17E-04	0.012
Haslinger_B_Cll_With_6q21_Deletion	17	-0.76538	-2.22106	<0.001	4.91E-04	0.015
Kegg_Type_I_Diabetes_Mellitus	18	-0.7293	-2.16346	<0.001	8.51E-04	0.027
Dalessio_Tsa_Response	21	-0.68454	-2.14132	<0.001	0.001259	0.041

Table S7. Biological processes downregulated in TT cells treated with 10nM Dinaciclib.

#pathway ID	pathway description	observed gene count	false discovery rate
GO.0006351	transcription, DNA-templated	248	1.28E-100
GO.0032774	RNA biosynthetic process	249	5.35E-97
GO.0034654	nucleobase-containing compound biosynthetic process	259	2.67E-96
GO.1903506	regulation of nucleic acid-templated transcription	262	3.49E-93
GO.0051252	regulation of RNA metabolic process	265	9.05E-93
GO.1901362	organic cyclic compound biosynthetic process	261	1.61E-92
GO.0006355	regulation of transcription, DNA-templated	261	1.71E-92
GO.0090304	nucleic acid metabolic process	282	2.77E-91
GO.2000112	regulation of cellular macromolecule biosynthetic process	270	5.67E-91
GO.0034645	cellular macromolecule biosynthetic process	272	1.28E-90
GO.0010556	regulation of macromolecule biosynthetic process	271	6.10E-90
GO.0010468	regulation of gene expression	277	1.71E-89
GO.0009059	macromolecule biosynthetic process	273	2.04E-89
GO.0044271	cellular nitrogen compound biosynthetic process	263	1.54E-88
GO.0019219	regulation of nucleobase-containing compound metabolic process	269	2.19E-88
GO.0006139	nucleobase-containing compound metabolic process	291	4.01E-87
GO.0000122	negative regulation of transcription from RNA polymerase II promoter	71	1.65E-23
GO.0007049	cell cycle	68	2.05E-09
GO.0000278	mitotic cell cycle	51	2.12E-09
GO.0044772	mitotic cell cycle phase transition	29	1.54E-08

Table S8. Biological processes upregulated in TT cells treated with 10nM Dinaciclib.

#pathway ID	pathway description	observed gene count	false discovery rate
GO.0032776	DNA methylation on cytosine	17	6.15E-34
GO.0000183	chromatin silencing at rDNA	17	1.68E-31
GO.0035574	histone H4-K20 demethylation	9	3.99E-17
GO.0006325	chromatin organization	22	4.04E-17
GO.0045653	negative regulation of megakaryocyte differentiation	9	1.45E-16
GO.0006334	nucleosome assembly	13	7.27E-16
GO.0006335	DNA replication-dependent nucleosome assembly	9	1.14E-15
GO.0031497	chromatin assembly	13	2.79E-15
GO.0051290	protein heterotetramerization	9	4.00E-15
GO.0051276	chromosome organization	22	1.42E-14
GO.0006323	DNA packaging	13	4.17E-14
GO.0034080	CENP-A containing nucleosome assembly	9	5.07E-13
GO.0061641	CENP-A containing chromatin organization	9	5.07E-13
GO.0034508	centromere complex assembly	9	1.18E-12
GO.0060968	regulation of gene silencing	8	2.07E-11
GO.0007264	small GTPase mediated signal transduction	17	6.96E-11
GO.0000723	telomere maintenance	9	7.90E-11
GO.0002682	regulation of immune system process	20	4.47E-09
GO.0002230	positive regulation of defense response to virus by host	8	2.30E-07
GO.0051172	negative regulation of nitrogen compound metabolic process	18	5.78E-07

Table S9. Biological processes downregulated MZ-CRC-1 cells treated with 20nM Dinaciclib.

#pathway ID	pathway description	observed gene count	false discovery rate
GO.0000278	mitotic cell cycle	141	9.01E-108
GO.1903047	mitotic cell cycle process	126	9.70E-95
GO.0022402	cell cycle process	133	1.18E-84
GO.0007049	cell cycle	145	3.36E-84
GO.0000082	G1/S transition of mitotic cell cycle	70	1.81E-77
GO.0044770	cell cycle phase transition	82	1.60E-73
GO.0044772	mitotic cell cycle phase transition	81	1.21E-72
GO.0051439	regulation of ubiquitin-protein ligase activity involved in mitotic cell cycle	40	1.96E-44
GO.0007093	mitotic cell cycle checkpoint	48	8.70E-44
GO.0031145	anaphase-promoting complex-dependent proteasomal ubiquitin-dependent protein catabolic process	38	2.54E-43
GO.0000075	cell cycle checkpoint	52	1.09E-42
GO.0051437	positive regulation of ubiquitin-protein ligase activity involved in regulation of mitotic cell cycle transition	36	1.34E-42
GO.1901990	regulation of mitotic cell cycle phase transition	54	1.36E-42
GO.0051726	regulation of cell cycle	89	1.82E-42
GO.0051436	negative regulation of ubiquitin-protein ligase activity involved in mitotic cell cycle	37	5.56E-42
GO.0006977	DNA damage response, signal transduction by p53 class mediator resulting in cell cycle arrest	34	7.15E-41
GO.1901991	negative regulation of mitotic cell cycle phase transition	45	1.07E-40
GO.0010948	negative regulation of cell cycle process	51	2.03E-40
GO.0031570	DNA integrity checkpoint	44	2.03E-40

Table S10. Biological processes upregulated in MZ-CRC-1 cells treated with 20nM Dinaciclib.

#pathway ID	pathway description	observed gene count	false discovery rate
GO.0032776	DNA methylation on cytosine	21	4.87E-43
GO.0000183	chromatin silencing at rDNA	21	1.60E-39
GO.0035574	histone H4-K20 demethylation	12	2.84E-24
GO.0045653	negative regulation of megakaryocyte differentiation	12	2.62E-23
GO.0006335	DNA replication-dependent nucleosome assembly	12	6.63E-22
GO.0051290	protein heterotetramerization	12	4.67E-21
GO.0006325	chromatin organization	26	2.58E-19
GO.0043486	histone exchange	13	8.54E-19
GO.0034080	CENP-A containing nucleosome assembly	12	5.76E-18
GO.0061641	CENP-A containing chromatin organization	12	5.76E-18
GO.0034508	centromere complex assembly	12	1.87E-17
GO.0006334	nucleosome assembly	14	3.08E-16
GO.0051276	chromosome organization	26	3.08E-16
GO.0031497	chromatin assembly	14	1.57E-15
GO.0006259	DNA metabolic process	23	5.17E-15
GO.0000723	telomere maintenance	12	6.02E-15
GO.0006323	DNA packaging	14	3.35E-14
GO.0007264	small GTPase mediated signal transduction	21	3.89E-13
GO.0060968	regulation of gene silencing	9	1.76E-12
GO.0002682	regulation of immune system process	24	4.05E-10

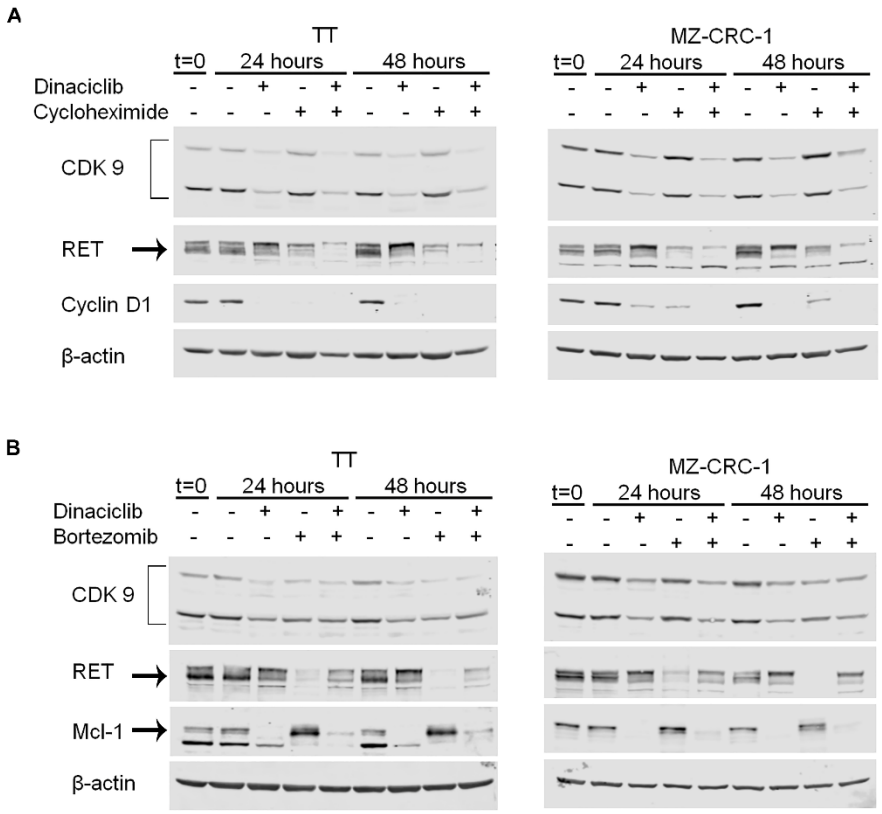

Figure S5. Effect of Dinaciclib treatment on CDK9 protein stability.
TT and MZ-CRC-1 cells were treated with **A.** Dinaciclib alone, cycloheximide alone, or co-treated with Dinaciclib and cycloheximide; or treated with **B.** Dinaciclib alone, bortezomib alone, or co-treated with Dinaciclib and bortezomib for 24h or 48h. After treatment, protein extracts were analyzed by Western blot for the level of CDK9, β-actin, and cyclin D1 or Mcl-1. Vehicle controls were collected for all time points in addition to a non-treated sample collected at the time that treatments were added for all experiments. Dinaciclib: 0.1μM, cycloheximide: 5.0μM, bortezomib: 0.1μM.

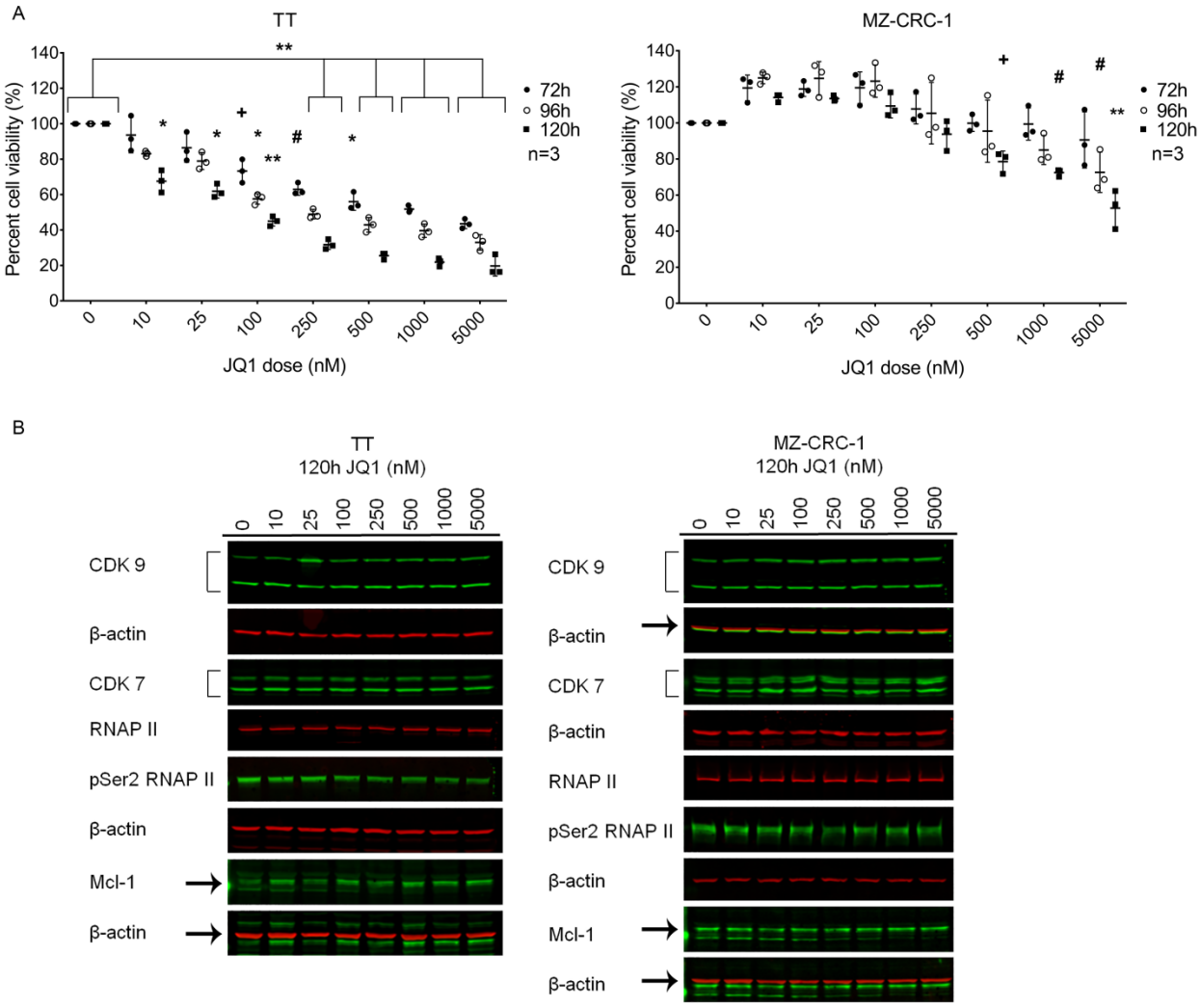

Figure S6. Effect of JQ1 treatment on TT and MZ-CRC-1 cell viability and CDK9 downstream pathway.

Cell viability assays (**A**) were performed with TT and MZ-CRC-1 cells treated with JQ1 or vehicle control. WST-8 solution was added at 72h-120h and the optical density was read using a spectrophotometer. These data were normalized to the 0nM (vehicle control) wells and represented as percentages. Each biological replicate was done in triplicate, and the error bars represent the standard deviation. Two-way ANOVA tests followed by Holm's procedure were done. **B**. Western blots performed with protein extracts from TT and MZ-CRC-1 cells treated with vehicle control or JQ1 for 120h showed that total CDK9 protein levels were not reduced with treatment, but there was a small downregulation of phosphorylation of RNA pol II at Ser2 on the TT cells. ** $P < 0.0001$, * $P < 0.001$, # $P < 0.01$, + $P < 0.05$.

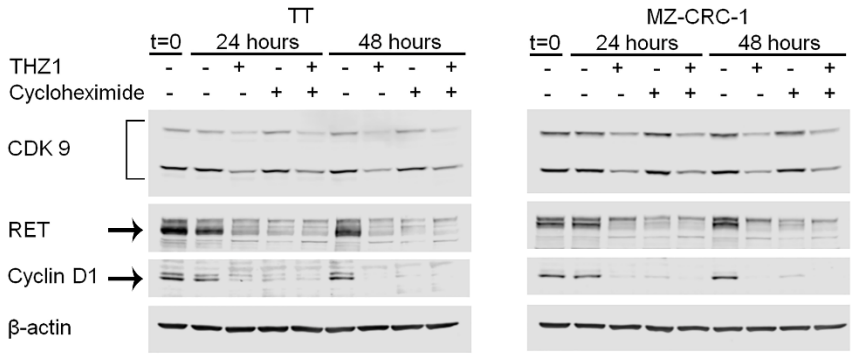

Figure S7. Effect of Dinaciclib treatment on CDK9 protein stability.
TT and MZ-CRC-1 cells were treated with THZ alone, cycloheximide alone, or co-treated with THZ1 and cycloheximide for 24h or 48h. After treatment, protein extracts were analyzed by Western blot for the level of CDK9, RET, β-actin, and cyclin D1. Vehicle controls were collected for all time points in addition to a non-treated sample collected at the time that treatments were added for all experiments. THZ1: 0.1μM (TT), 0.25μM (MZ-CRC-1), cycloheximide: 5.0μM.

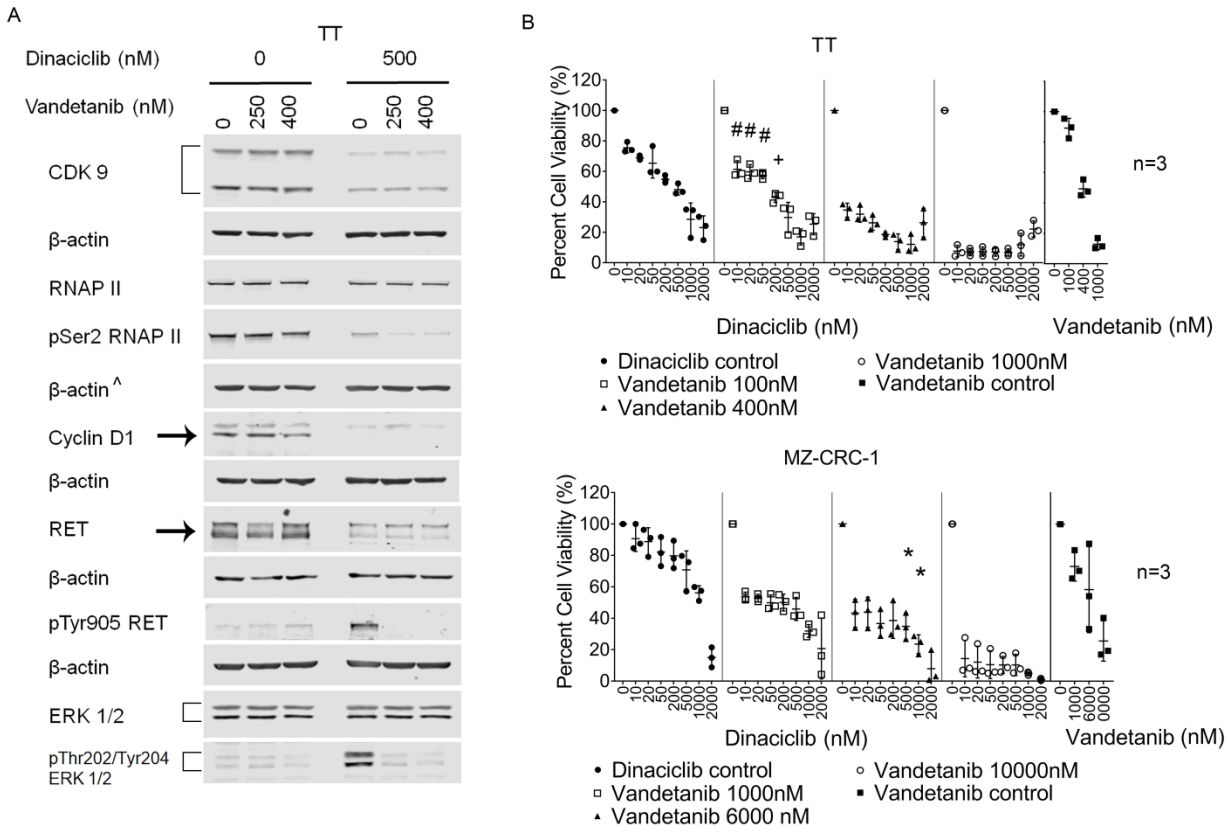

Figure S8. Effect of Dinaciclib-Vandetanib combination therapy on MTC cells *in vitro.*
TT and MZ-CRC-1 cells were treated with Dinaciclib for 6h and incubated in 2% FBS- RPMI medium for 72h (Dinaciclib control), or Vandetanib alone for 72h (Vandetanib control), or Dinaciclib for 6h followed by 72h of Vandetanib incubation. Dinaciclib treatment induced RET and ERK activation, which was obliterated by Vandetanib treatment (**A**). Cell viability assays showed synergistic effect between these drugs in both cell lines (**B**). Linear mixed models were used to statistically analyze the cell viability. If the difference of the optical density ((combination-Dinaciclib)-(Vandetanib –control)) <0 and the p-value is significant, then we claimed there is significant synergistic interaction at the tested dose. * $P < 0.001$, # $P < 0.01$, + $P < 0.05$. ^β-actin for RNAP II, pSer2 RNAP II, ERK 1/2, and pThr202/Tyr204 ERK 1/2 in this figure is the same because they were blotted in the same membrane.

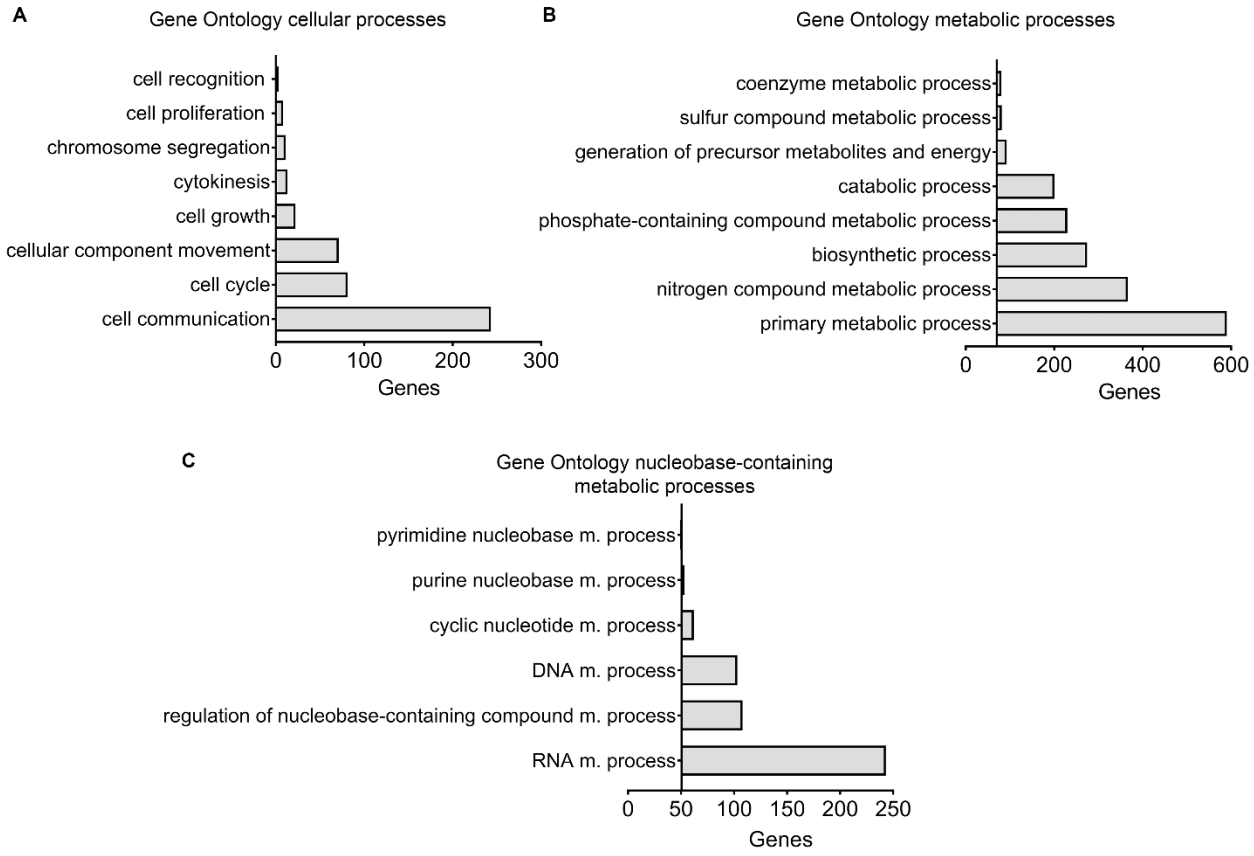

Figure S9. Gene Ontology cellular and metabolic processes associated with super-enhancers identified in the TT cell line.

ChIP sequencing was performed on TT cells looking at H3K27Ac and BRD4 binding sites. The genes associated with super-enhancers were loaded to PANTHER to identify the biological processes associated. The two highest categories within biological processes were cellular (**A**) and metabolic (**B**) processes, which in turn contain sub-categories shown here. Among these processes, cell communication and primary metabolic processes are associated with the highest number of genes. Out of the primary metabolic processes, nucleobase-containing compound metabolic processes (**C**) stand out, with RNA processes accounting for the most genes in this category.

Table S11. Array-CGH analysis of CDK9 in human MTCs

	Patient number	*RET* mutation	Lymph node metastases present	Distant metastases present	CDK9 copy number
Sporadic MTC without RET mutation	1	n/a	Yes	No	3
	2	n/a	Yes	No	2
	3	n/a	Yes	No	3
	4	n/a	Yes	No	2
	5	n/a	Yes	No	2
	6	n/a	Yes	No	2
	7	n/a	No	No	2
	8	n/a	No	No	2
	9	n/a	No	No	3
	10	n/a	No	No	3
Sporadic MTC with somatic RET mutation	11	918	Yes	Yes	3
	12	918	Yes	Yes	2
	13	918	Yes	Yes	3
	14	918	Yes	Yes	2
	15	918	Yes	Yes	2
	16	918	Yes	No	2
	17	883	Yes	No	2
	18	898	Yes	No	2
	19	918	No	No	3
	20	918	No	No	3
Hereditary MTC with germline RET mutation	21	620	Yes	Yes	2
	22	634	Yes	Yes	3
	23	918	No	Yes	2
	24	634	Yes	No	2
	25	634	Yes	No	2
	26	634	Yes	No	4
	27	918	Yes	No	3
	28	918	No	No	2
	29	918	No information	No information	2
	30	804	No information	No information	2

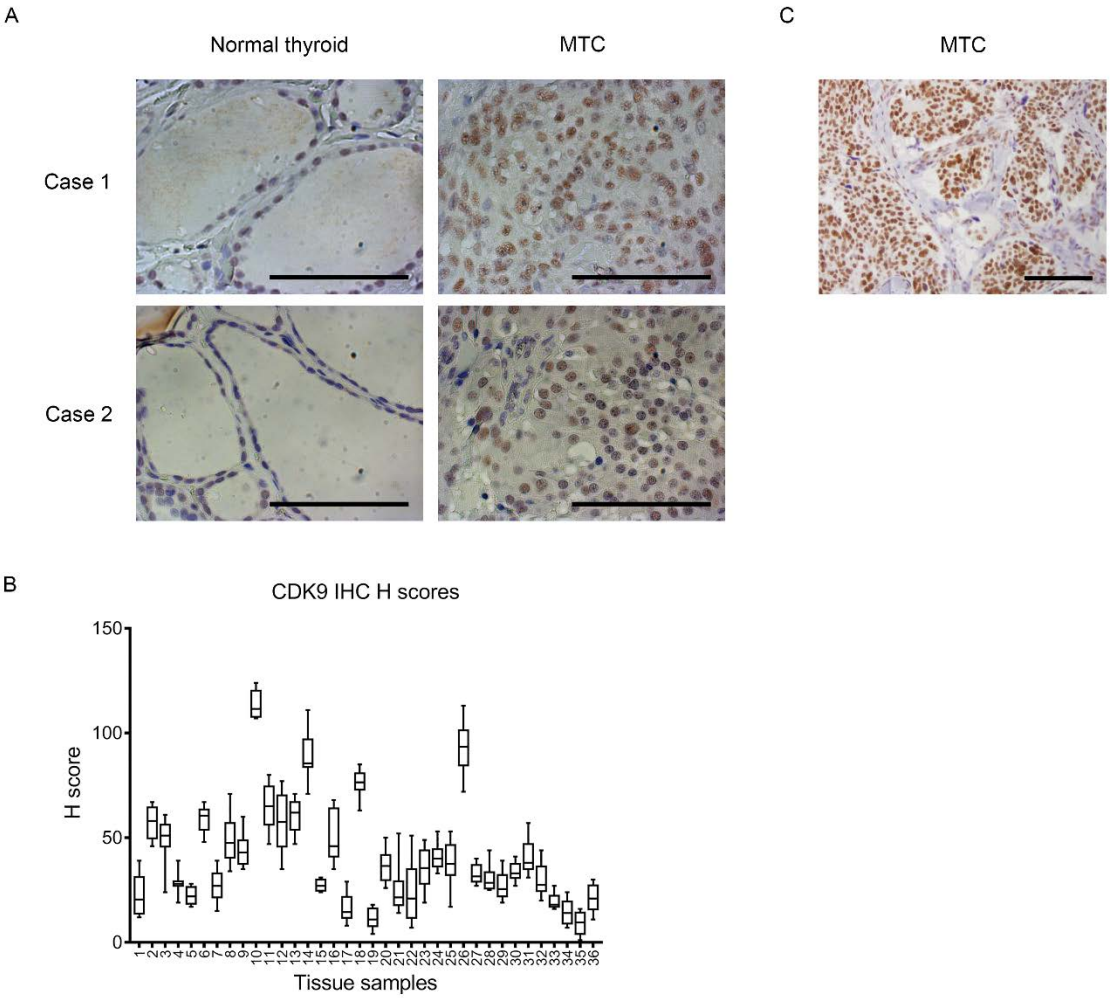

Figure S10. CDK9 expression in MTC human samples.
A. Paraffin-embedded tissue samples from 14 MTC patients were immunostained for CDK9. 10 out of 14 cases had stronger staining in the tumor area vs. the normal thyroid. Two cases are represented. Scale bar indicates 100µm, magnification: 400X. **B.** An additional 36 cases were immunostained for CDK9 and quantified using the Vectra Automated Quantitative Pathology Imaging System, generating H scores for each field of view (10 per slide). The graph represents the mean H scores per slide. These cases did not have normal thyroid areas. **C.** A representative image of a separate cohort of 65 MTC tumor microarrays which were immunostained for CDK9. Scale bar indicates 100µm, magnification: 200X.